Creep Deformation of Alumina–SiC Composites

S. R. NUTT and P. LIPETZKY

Division of Engineering, Brown University, Providence, RI 02912 (U.S.A)

P. F. BECHER

Oak Ridge National Laboratory, Metals and Ceramics Division, Oak Ridge, TN 37831 (U.S.A.)

(Received April 21, 1989)

Abstract

Composites of alumina reinforced with SiC whiskers have been creep tested in bending and in compression at 1200–1400 °C in an air ambient. The flexural creep data follow a power law constitutive relation with two distinct stress exponents that depend on the level of applied stress. Crept specimens were examined by transmission electron microscopy to determine the mechanisms of creep deformation and microstructural damage. The primary mechanism of creep deformation under these conditions is grain boundary and interface sliding resulting from diffusion. At high stress levels, the sliding is often unaccommodated, resulting in cavitation at grain boundary–interface junctions. Cavitation is associated with an increase in the stress exponent for flexural creep.

1. Introduction

Ceramic composites have emerged as an important class of materials for high temperature structural applications because of the ever-increasing demand for materials that can withstand more severe environmental conditions. The mechanical properties of composites at elevated temperatures depend on the properties of the constituents, the distribution and morphology of these phases, and the properties of the interface between the phases. Creep resistance is often the most critical high temperature property of ceramics, and it is often the major limitation for high temperature applications. Under creep conditions, the mechanical response of the composite is strongly affected by the presence of the reinforcing phase and the strength of the interfacial bond between the matrix and the reinforcement. Creep damage of the composite can result in microscopic cavities and cracks that reduce the load-bearing capacity of the component and eventually cause failure. Before ceramic composites can be used reliably in structural applications at elevated temperatures, the mechanisms of damage and deformation that occur during creep must be understood. The objective of the present study is to investigate the creep response of a model ceramic composite, using transmission electron microscopy (TEM) observations of crept specimens to determine the mechanisms of deformation and damage.

One of the most widely studied ceramic composites consists of an alumina matrix reinforced with SiC whiskers. The addition of SiC reinforcements results in substantial improvements in room temperature toughness [1–3] and increased resistance to erosion and thermal shock [4]. Commercial applications of these materials include cutting tools, valve and pump components, and extrusion dies. The composites are typically fabricated by hot pressing a high purity alumina powder blended with short single-crystal fibers (whiskers) of SiC in volume fractions ranging from 0.15 to 0.35. The whiskers tend to lie perpendicular to the hot-pressing axis (HPA), and whisker aspect ratios are typically 5–10 in the fabricated composites. While most research has focused on the room temperature properties of these composites, there is increasing interest in high temperature behavior. Early work by Chokshi and Porter [5] demonstrated a substantial improvement in creep resistance when alumina was reinforced with SiC whiskers. Furthermore, they concluded that the applied stress was carried largely by the whisker reinforcements and that the creep response of the whiskers appeared to control the creep of the composite. Their work demonstrated a need to

0921-5093/90/$3.50

understand the creep deformation mechanisms in composites better and to determine the role of microstructural parameters during creep.

2. Experimental procedure

The composite material selected for this study consisted of a polycrystalline alumina matrix reinforced with SiC whiskers, manufactured by the Greenleaf Corporation (WG-300). Microstructural characterization of the as-fabricated composites showed an average grain size of 1–2 μm and a reinforcement volume fraction of 0.33. Sintering additives such as yttria and magnesia are often used to facilitate densification of alumina ceramics. These additives often result in pockets of residual glass phase at triple-grain junctions and, in composites, at grain boundary–interface junctions. However, the as-fabricated composite material was exceptional in that accumulations of glass phase were not detected at boundary junctions except in rare instances. The primary processing defect in as-fabricated composites consisted of whisker-free channels of matrix material, as shown in Fig. 1, an image of a polished surface of the composite parallel to the HPA. The observed macrostructure is probably associated with a granulation process used to produce controlled agglomerates of alumina powder and SiC whiskers prior to hot pressing. Segregation of finer particles to granule surfaces is not an uncommon phenomenon during drying [6], and this segregation would result in granules having alumina-rich surfaces. If, after pressing, these alumina-rich regions were retained, they would be manifest in the type of macrostructure shown in Fig. 1.

Flexural and compressive creep tests were conducted in air at temperatures of 1200–1400 °C. Flexural creep specimens (2.5 mm × 5 mm × 51 mm) were loaded in a four-point bending fixture in which the load points and support points were separated by 19 mm and 38 mm respectively. Before application of a constant load, specimens were heated to the test temperature and held for 30 min to allow the apparatus to equilibrate. The displacement of the center of the specimen relative to the load pins was monitored with a linear variable-differential transducer and recorded.

The applied stresses and resultant strains were determined using the method described by Hollenberg *et al.* [7], in which the deflection of the specimen is assumed to be sufficiently small that the stresses can be predicted by linear elastic beam theory. In most tests, the maximum strain was limited to less than 0.3%, thus ensuring that the stress gradient through the bend bar remained approximately constant and that a nearly constant stress was applied to the tensile surface throughout the test. Secondary creep rates were estimated from minimum creep rates in tests taken into the tertiary creep stage, and from similar tests interrupted during earlier stages of secondary creep. Test specimens were cooled under load to preserve the crept microstructures for subsequent TEM characterization.

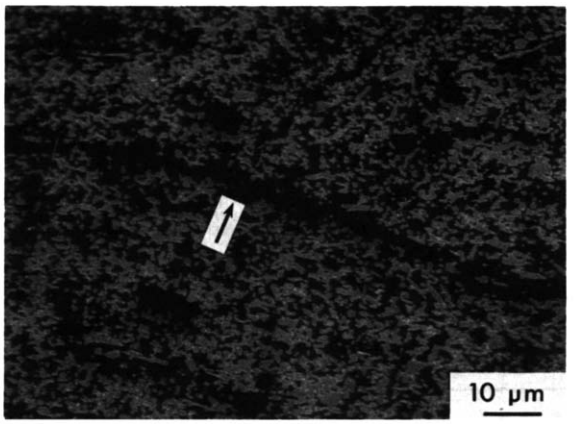

Fig. 1. Non-uniform whisker distribution seen in a transverse section of a hot-pressed composite plate. The arrow indicates a whisker-free channel.

Compression tests were conducted in an air ambient under a constant applied stress using an apparatus described previously [8]. Cylindrical specimens 4 mm in diameter and 6 mm in length were ground and polished prior to testing. Creep tests were conducted at 1200–1400 °C under applied stresses of 25–175 MPa. After testing, the density of selected specimens was measured to determine the amount of cavitation that had occurred.

TEM specimens were prepared from crept specimens by cutting sections perpendicular to the cylinder axis. Tests were generally interrupted during the secondary stage of creep and cooled under load before sectioning. Disks were cut and mechanically thinned before ion milling to perforation. Specimens were examined in an analytical transmission electron microscope operated at 120 kV and equipped with a double-tilt specimen holder.

3. Results and discussion

3.1. Flexural creep

Flexural creep data typically showed primary, secondary and tertiary stages of creep. Some of these data are summarized in Fig. 2, a plot of the secondary creep rate *vs.* outer-fiber stress for a range of stress levels at 1200 and 1300 °C. The data sets for both temperatures are bilinear and exhibit slopes of approximately 1 for low stress levels (regime I) and 5 for higher stress levels (regime II). On the assumption of a power law constitutive relation between the secondary creep rate and the applied stress (in which the creep rate is proportional to the applied stress raised to an exponent n), the slopes in Fig. 1 yield values for the stress exponent n. The pronounced change in the slope reflects the onset of a different deformation mechanism associated with higher stress levels. For a given stress level, an increase in temperature causes an increase in creep rate. However, for both temperatures, an increment in stress causes an equivalent increase in creep rate, provided that the stress regime remains unchanged.

For creep of fine-grain alumina and other ceramics, stress exponents of 1–2 have generally been associated with a diffusional creep mechanism [9, 10], and it is not unreasonable to suppose that the composite material tested here deforms by a similar mechanism at low stress levels (regime I). However, creep deformation mechanisms cannot be reliably inferred from stress exponent values for multiphase materials, particularly composites. Chokshi and Porter [5] conducted flexural creep tests on similar composite material and reported a stress exponent of 5.2 for temperatures of 1500–1600 °C and concluded that the operative creep mechanism was intragranular glide of dislocations. While the stress exponent value measured in our tests at high stress levels ($n = 5$) is virtually identical with the value reported by Chokshi and Porter, our TEM observations indicate that dislocation glide plays an insignificant role in creep at 1200–1300 °C.

Secondary creep rates measured at different temperatures are plotted against inverse absolute temperature in Fig. 3, yielding activation energies of approximately 300 kJ mol^{-1}. The measured values are significantly lower than those reported previously by Chokshi and Porter [5], who measured an activation energy of 450 kJ mol^{-1} for flexural creep at 1500–1600 °C. The difference in activation energy is attributed to a different deformation mechanism operative at the lower test temperatures used in the present study. In addition to the difference in activation energies, the measured strain rates for a given temperature and stress level were substantially lower than the creep rates reported by Chokshi and Porter. The whisker volume fraction in materials studied here was twice as great as the whisker volume fraction in their material, accounting for the large difference in strain rates for comparable stress levels.

3.2. Compressive creep

Creep tests were also conducted under constant compressive stresses in air at from

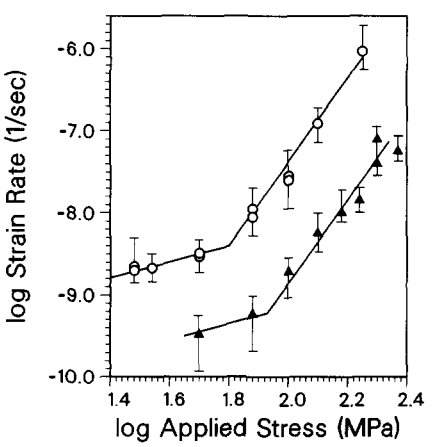

Fig. 2. Strain rate *vs.* stress relations for flexural creep of SiC-reinforced alumina composites: ▲, 1200 °C; ○, 1300 °C. The bilinear behavior yields stress exponents of $n = 1$ and $n = 5$, assuming a power-law-type constitutive relation.

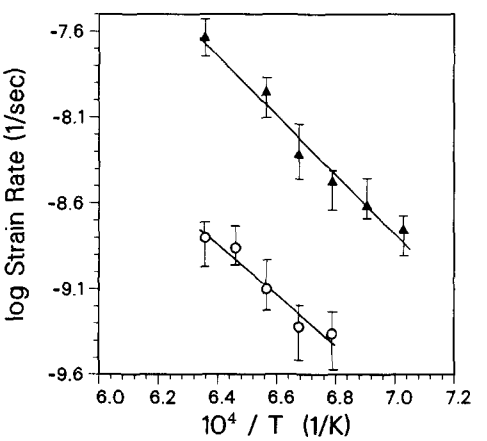

Fig. 3. Arrhenius plot of minimum creep rate *vs.* inverse temperature for composite deformed in bending under an applied stress of 50 and 100 MPa (○, 50 MPa; ▲, 100 MPa; air ambient).

1200 to 1400 °C with stress levels ranging from 25 to 175 MPa. The results are summarized in Fig. 4(a), a log–log plot of creep rate *vs.* applied stress. The data are approximately linear on the log–log plot, implying power-law-type constitutive behavior. The stress exponent is approximately 3 for both temperatures, although one data point at 1400 °C suggests that the stress exponent may shift to a value of 1 at low stress levels. This shift would be similar to the creep response observed in bending and might indicate a different deformation mechanism at lower stress levels.

Figure 4(b) shows an Arrhenius plot of minimum creep rate *vs.* inverse temperature for compression of the alumina–SiC composite. The plot yields activation energies of 270 kJ mol^{-1} for temperatures below 1270 °C, and 655 kJ mol^{-1} for higher temperatures. These data imply a thermally activated creep deformation mechanism that becomes operative above 1270 °C. Identification of the activated mechanism requires careful TEM characterization of crept specimens, currently in progress.

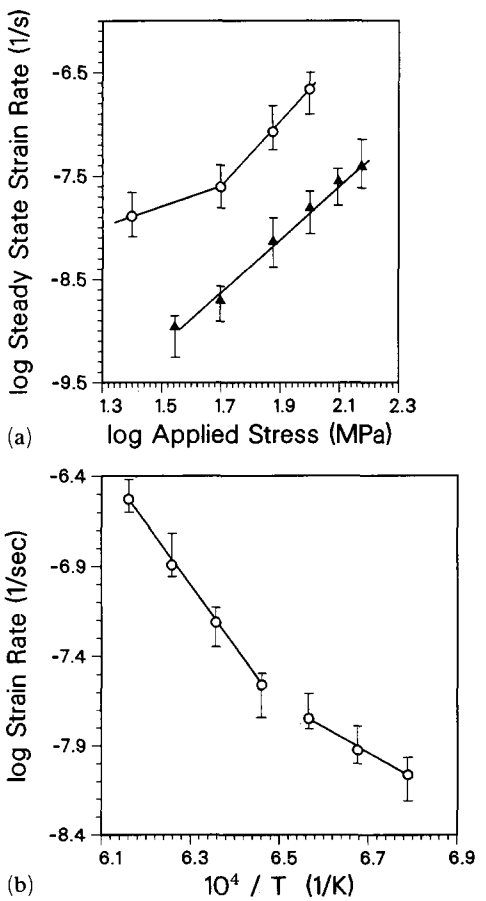

Fig. 4. Compressive creep of alumina–SiC composites in air ambient: (a) strain rate *vs.* stress relations: ▲, 1300 °C; ○, 1400 °C. (b) Arrhenius plot of minimum creep rate *vs.* inverse temperature (stress, 150 MPa).

The creep data for compression can be compared with the data obtained in bending. The values of the stress exponent measured in compression ($n = 3$) are similar to those measured for flexural creep tests ($n = 5$), suggesting that similar creep deformation mechanisms may operate in bending and in compression at these temperatures. However, the strain rates for compression are much lower than in bending for comparable stress levels. Creep rates for ceramics are generally lower in compression than in tension or bending [11]. Furthermore, bending necessarily involves substantial stress concentrations beneath the loading pins that can cause localized deformation and result in higher measured strains.

3.3. Creep deformation mechanisms

Flexural creep specimens that had reached secondary creep under low levels of applied stress resulted in a stress exponent n of 1, and these were examined by TEM. The most salient microstructural change was the development of pockets of silica glass phase at grain boundary–interface junctions (Fig. 5). Compositional analysis by X-ray spectroscopy revealed the presence of silicon with trace amounts of calcium or sulfur, from which it was concluded that the glass phase was predominantly silica. (Calcium is the major impurity in the as-grown whiskers [12], and the calcium may originate from within the whiskers.) Similar glass pockets were also observed at triple-grain junctions, although with less frequency, and calcium was generally not present in these pockets. The dislocation density was negligible, supporting the likelihood of a diffusional creep deformation mechanism in this stress–temperature regime.

Flexural specimens crept at higher stress levels (yielding stress exponent values of $n = 5$) contained cavities at grain boundary–interface junctions. Figure 6 shows a typical cavity formed at a whisker interface intersected by a grain boundary. The cavities were typically on the order of one hundred nanometers, which is consistent with the size of cavity predicted by the diffusional creep model developed by Cannon *et al.* [13]. The cavities were triangular and were usually lined with a thin film of silica glass. Incipient cavities, consisting of glass pockets containing small bubbles, were also observed along whisker inter-

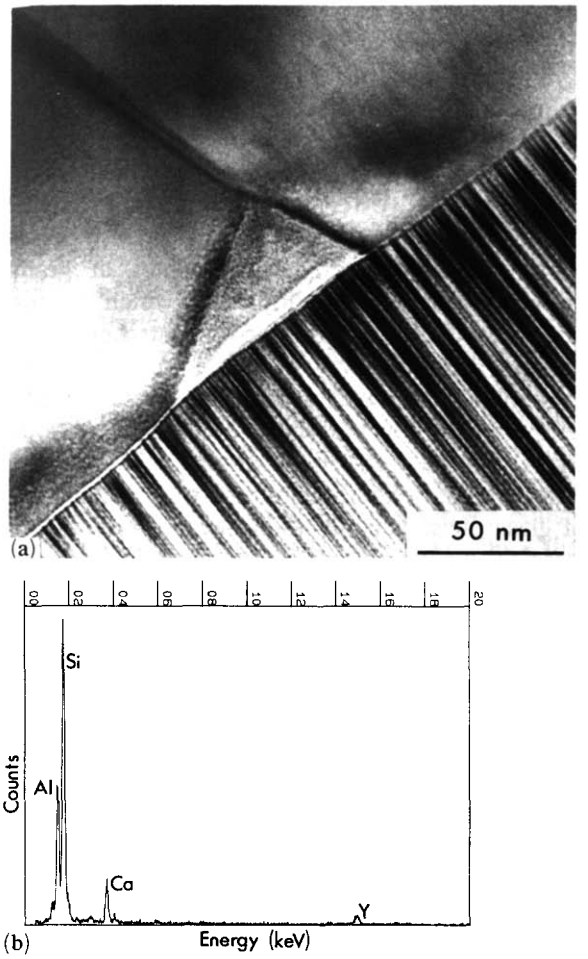

Fig. 5. (a) Accumulation of non-crystalline silica phase at a grain boundary–interface junction after secondary creep in regime I; (b) X-ray spectrum from triangular region showing primarily silicon.

faces, from which it was concluded that cavitation was generally preceded by the accumulation of glass phase. Cavities were less frequently observed along triple-grain junctions and along grain boundaries, and grain boundary glass films were detected. The viscosity of silica glass is reduced to about 10 P at temperatures of 1200–1300 °C, and the viscosity is further reduced by the presence of impurities such as calcium [14]. Thus the viscous flow of glass phase during composite creep constitutes an important deformation mechanism that also facilitates interfacial and intergranular sliding and cavitation.

In addition to the microstructural changes noted above, corrugated grain boundaries were observed, as shown in Fig. 7. Heuer *et al.* [15] have determined that corrugated grain boundaries in alumina arise during diffusional creep

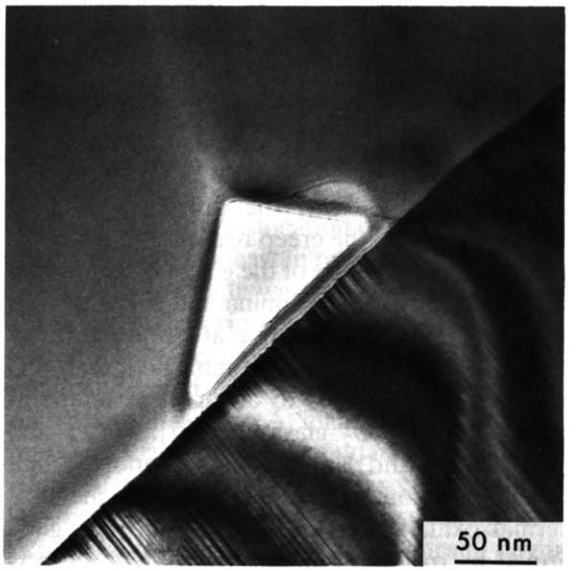

Fig. 6. Cavity formation at grain boundary–interface junction in composite after secondary creep at 1300 °C in regime II.

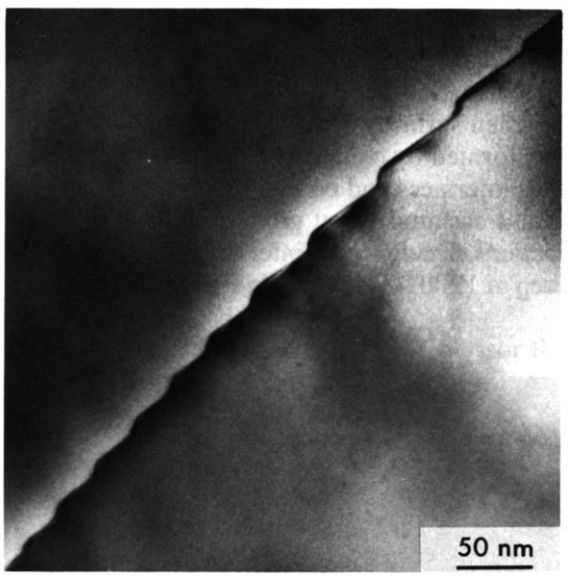

Fig. 7. Corrugated grain boundary in flexural specimen after secondary creep at 1300 °C under stress of 50 MPa.

because of unaccommodated grain boundary sliding (a dissolution–precipitation reaction) [15]. The dislocation density was negligible and, although intragranular dislocations and small-angle grain boundaries were occasionally observed, these features were also present in the material prior to testing. The relative importance of dislocation glide as a creep deformation mechanism in this material under these conditions was concluded to be small.

The marked change in stress exponent that occurs as the stress level is increased (see Fig. 2) is associated with an incremental increase in cavitational strain. Microstructural observations indicate that cavitation is preceded by the accumulation of glass phase at grain boundary–interface junctions. Clearly, the presence of glass phase is critical to the creep response of the composite, and the origin(s) of the glass phase must be considered. Although alumina and SiC show no evidence of chemical reaction at temperatures of 1200–1300 °C, it is well established that SiC oxidizes when exposed to air at these temperatures, forming SiO_2 glass [16, 17]. Porter and Chokshi [18] and Lin *et al.* [19] reported that alumina–SiC composites undergo a topochemical thermal oxidation reaction in which silica glass formed by oxidation of SiC subsequently reacts with alumina to form a mullite surface scale. Surface scales 5–10 μm thick were generally present after creep testing, and the scales consisted primarily of mullite and residual silica glass.

It appears that much of the silica glass that accumulates at interfaces during creep results from oxidation of SiC whiskers at and near the specimen surfaces. Under load, the low viscosity glass formed by oxidation of SiC then penetrates along interfaces and boundaries into the composite and accumulates at grain boundary–interface junctions. Evidence of interface glass films after creep at 1200 °C is shown in Fig. 8, a high resolution TEM image of a whisker side, viewed edge on. The thickness of the glass film is about 0.75–1 nm, and the thickness increases where grain boundaries intersect the interface. Sections taken from regions exposed to tensile stress generally show more glass phase than those taken from compressive regions, implying that tensile stress on boundaries facilitates glass phase penetration. Glassy material accumulates at grain boundary–interface junctions, after which cavities nucleate and grow, permitting the matrix grains to debond and pull away from the whisker. TEM examination of specimens exposed to similar temperatures for the same times (but without stress) showed glass films along interfaces and grain boundaries, although there was no evidence of glass phase accumulation at grain boundary–interface junctions.

Evidence of subsurface oxidation of SiC whiskers is shown in Fig. 9, a TEM image showing a subsurface whisker that was located near the surface of an oxidized specimen. The whisker is partially oxidized, resulting in the formation of silica glass (G) and graphitic carbon (C). As the oxidation reaction proceeds, the graphitic carbon is oxidized to form CO_2 and, at sufficiently high temperatures, the silica glass can react with the adjoining alumina to form crystalline mullite or possibly other aluminosilicate phases [18, 19]. The silica glass formed by the thermal oxidation reaction is believed to infiltrate the material during creep, leading to glass phase accumulation and cavitation at grain boundary–interface junctions. Details of the oxidation reaction mechanisms and kinetics have been reported in ref. 19.

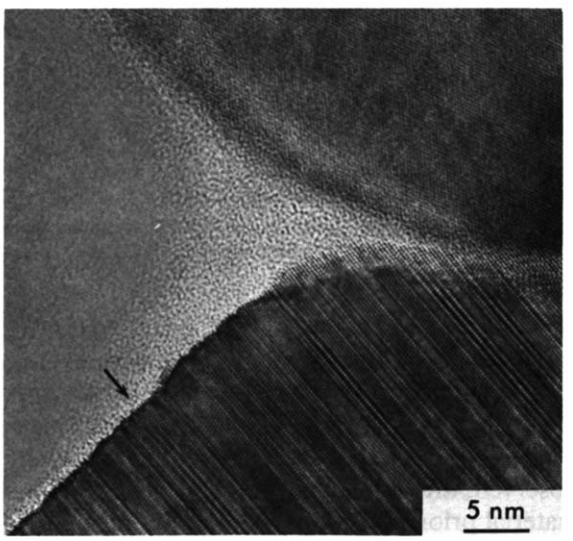

Fig. 8. Accumulation of silica glass phase at grain boundary–interface junction after flexural creep at 1300 °C and 150 MPa. The arrow indicates the glassy film along the SiC–alumina interface.

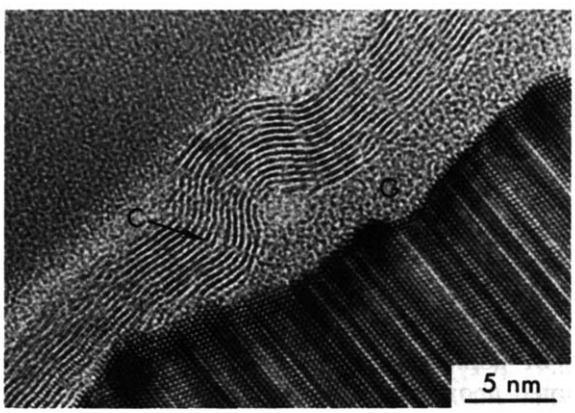

Fig. 9. Subsurface oxidation of SiC whisker after flexural creep at 1300 °C. The reaction produces graphitic carbon (C) and silica glass (G), which subsequently penetrates the material via migration along boundaries.

The possible source(s) of glass phase in crept specimens include glass phase present in the as-fabricated material, henceforth referred to as prior glass phase. High resolution TEM images of as-fabricated material show that extremely thin non-crystalline films (0.5–0.7 nm thick) are detectable along some whisker interfaces (Fig. 10). This observation suggests that redistribution of prior glass phase constitutes a secondary source of the glass phase observed in crept specimens. Furthermore, recent creep experiments conducted in oxygen-free ambients indicate that some redistribution of prior glass phase does indeed occur during creep, and can result in glass phase pockets at grain boundary–interface junctions [20]. These observations indicate that thermal oxidation of SiC at and near the surface constitutes the primary source of the glass phase that develops at grain boundary–interface junctions during creep in air ambients, while the prior glass phase is probably a secondary source. The relative contributions of these sources is presently undetermined, although controlled-atmosphere creep experiments should yield more quantitative indications.

4. Summarizing remarks

Flexural and compressive creep tests were performed in air on alumina reinforced with 33 vol.% SiC whiskers at 1200–1400 °C. In flexure, increasing the applied stress above a critical value caused the measured stress exponent for secondary creep to change from $n = 1$ to $n = 5$, while in compression the measured stress exponent was approximately $n = 3$. TEM observations of crept specimens cooled under load revealed accumulations of silica glass phase at internal boundary junctions and low dislocation densities. The silica glass originated at least in part from the oxidation of SiC whiskers. It was concluded that at low stress levels the primary deformation mechanism was diffusional creep and grain boundary sliding, facilitated by viscous flow of intergranular and interfacial silica glass. At higher stress levels, cavitation occurred at grain boundary–interface junctions, enabling matrix grains to separate from the whiskers and causing an increase in the stress exponent. With increasing creep strain, cavities linked together and formed cracks which eventually caused failure. Density measurements showed that the cavitational component of the total flexural creep strain increased substantially above a stress level of about 70 MPa, indicating that an increase in cavitation was responsible for the increase in stress exponent observed at higher stress levels.

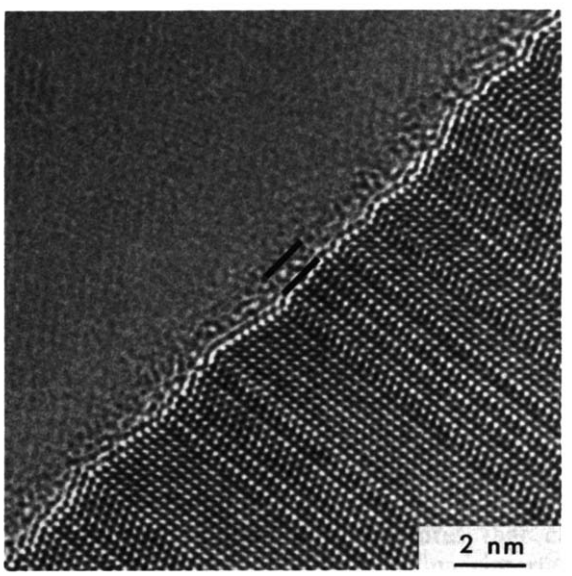

Fig. 10. Non-crystalline film at interface between SiC whisker and alumina matrix in as-fabricated composite. Planar defects in the whisker (microtwins and stacking faults) give rise to the chevron appearance of the lattice fringes [12].

Acknowledgments

Support from the Office of Naval Research through Contract N00014-86-K-0125 is gratefully acknowledged.

The authors also wish to thank Professor R. F. Davis for access to his laboratory and D. Koester for assistance with compressive creep testing.

References

1 P. F. Becher and G. C. Wei, *J. Am. Ceram. Soc.*, *67* (1984) C267.
2 K. T. Faber and A. G. Evans, *Acta Metall.*, *31* (1983) 565.
3 A. Morrone, S. Nutt and S. Suresh, *J. Mater. Sci.*, *23* (1988) 3206.
4 T. N. Tiegs and P. F. Becher, *J. Am. Ceram. Soc.*, *70* (1987) C109.
5 A. H. Chokshi and J. R. Porter, *J. Am. Ceram. Soc.*, *68* (1985) C144.
6 J. S. Reed, *Introduction to the Principles of Ceramic Processing*, Wiley, New York, 1988, p. 323.
7 G. W. Hollenberg, G. R. Terwilliger and R. S. Gordon, *J. Am. Ceram. Soc.*, *54* (1971) 196.
8 C. H. Carter, Jr., C. A. Stone, R. F. Davis and D. R. Schaub, *Rev. Sci. Instrum.*, *51* (1980) 1352.
9 W. R. Cannon and T. G. Langdon, *J. Mater. Sci.*, *23* (1988) 1.

10 W. R. Cannon and R. L. Coble, in R. C. Bradt and R. E. Tressler (eds.), *Deformation of Ceramic Materials*, Plenum, New York, 1975, pp. 61–100.
11 S. M. Wiederhorn, S. M. Roberts, T.-J. Chuang and L. Chuck, *J. Am. Ceram. Soc., 71* (1988) 602.
12 S. R. Nutt, *J. Am. Ceram. Soc., 71* (1988) 149.
13 W. R. Cannon, W. H. Rhodes and A. H. Heuer, *J. Am. Ceram. Soc., 63* (1980) 46.
14 R. H. Doremus, *Glass Structure*, Wiley, New York, 1973, p. 105.
15 A. H. Heuer, N. J. Tighe and R. M. Cannon, *J. Am. Ceram. Soc., 63* (1980) 53.
16 J. A. Costello and R. E. Tressler, *J. Am. Ceram. Soc., 69* (1986) 674.
17 C. D. Fung and J. J. Kopanski, *Appl. Phys. Lett., 45* (1984) 757.
18 J. R. Porter and A. H. Chokshi, in J. A. Pask and A. G. Evans (eds.), *Ceramic Microstructures: 1986*, Plenum, New York, 1988, p. 113.
19 F. Lin, T. Marieb, A. Morrone and S. Nutt in F. D. Lemhey, S. G. Fishman, A. G. Evans and J. R. Strife (eds.), *High Temperature/High Performance Composites, Materials Research Society Symp. Proc.*, Vol. 120, Materials Research Society, Pittsburgh, PA, 1988, p. 323.
20 P. Lipetzky, S. R. Nutt, R. F. Davis and D. Koester, unpublished results, 1990.